Supporting Information

Accessing the Band Structure of Perovskite Solar Cells: Photoelectron Spectroscopy and 2D Modeling of Tapered Cross Section

*Clemens Baretzky, Clément Maheu, Markus Frericks, Thomas Mayer, Uli Würfel**

C. Baretzky, U. Würfel
Fraunhofer Institute for Solar Energy Systems ISE,
Heidenhofstraße 2, 79110 Freiburg, Germany.

C. Baretzky, U. Würfel
Freiburg Materials Research Center FMF, University of Freiburg,
Stefan-Meier-Straße 21, 79104 Freiburg, Germany.

C. Maheu, T. Mayer
Surface Science Laboratory, Department of Materials and Earth Sciences, Technical University of Darmstadt,
Otto-Berndt-Strasse 3, 64287 Darmstadt, Germany

E-mail: uli.wuerfel@ise.fraunhofer.de

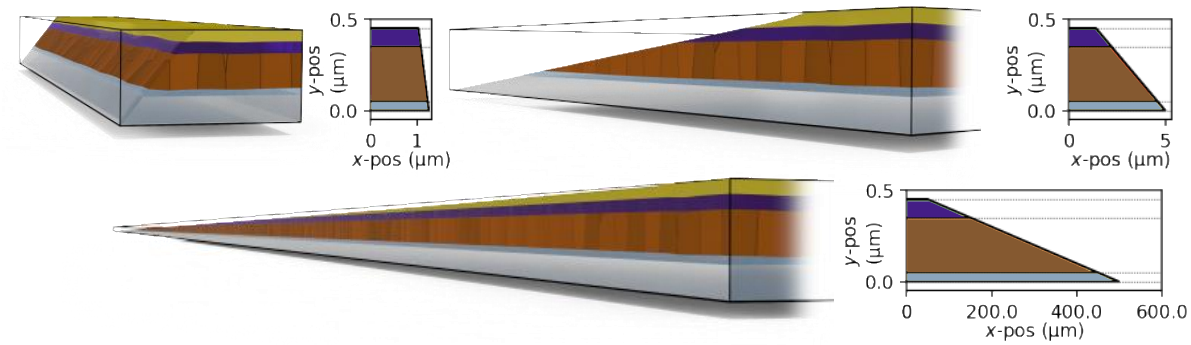

Figure S1: Sketch to convey the actual aspect ratio of the investigated TCS with corresponding layer cut. The bottom image corresponds to a device with a tapered width of 440 µm which is still shy of the investigated device with a tapered width of 3000 µm. The colors in the graphs correspond to Spiro-OMeTAD (purple), Perovskite (brown) and FTO (grey).

Section S1: Experimental Details:

The structure of the investigated PSC is depicted in **Figure 1** with Au | Spiro-OMeTAD | Perovskite | m-TiO_2 | c-TiO_2 | SnO_2 layers. Details about the solar cell fabrication can be found elsewhere.[S1] The sample was polished with a metallographic polishing machine on a silk cloth (type 9450) at 80 rpm. The polishing procedure was conducted under an ambient atmosphere applying a small angle (estimated to be roughly 0.02°) to create a TCS.

A Thermo Fischer VG Escalab 250 spectrometer with an Al-Kα source (1486.6 eV) at a pass energy of 10 eV was used to perform PES measurements. The X-ray spot size was estimated to be 250 µm in diameter. XPS line scans over the tapered part of the sample were performed with a step width of 50 µm along the 3 mm TCS. The size of the tapering angle has been deduced by knowing the size of the normal part (roughly 1 µm) and the size of the tapered width (roughly 3 mm) *i.e.* the distance between the top Au contact and the bottom FTO substrate detected by XPS.

$$\text{Tapering angle} = \tan^{-1}\left(\frac{\text{Normal part width}}{\text{Tapered width}}\right) \quad \text{(S1.1)}$$

To perform a second PES measurement under illumination we used a 50 W ECONLUX SolarRaptor tungsten high-intensity discharge lamp attached to one of the glass view ports of the XPS measurement chamber and the sample was illuminated from roughly 50 cm at an angle of around 45°. Given the power of the lamp P_{Lamp} of 50 W, the distance to the sample r of 50 cm and the cone angle of 23°, the power density at the sample

$$P_{\text{Sample}} = P_{\text{Lamp}}/(4\pi r^2(1-\cos 23°))\cos 45°$$

should be at maximum 140 W/m^2, thus, well below AM1.5G. Given the additional losses in efficiency and transmission, the true power is probably still significantly lower, reasonably within the 30 W estimated from simulations.

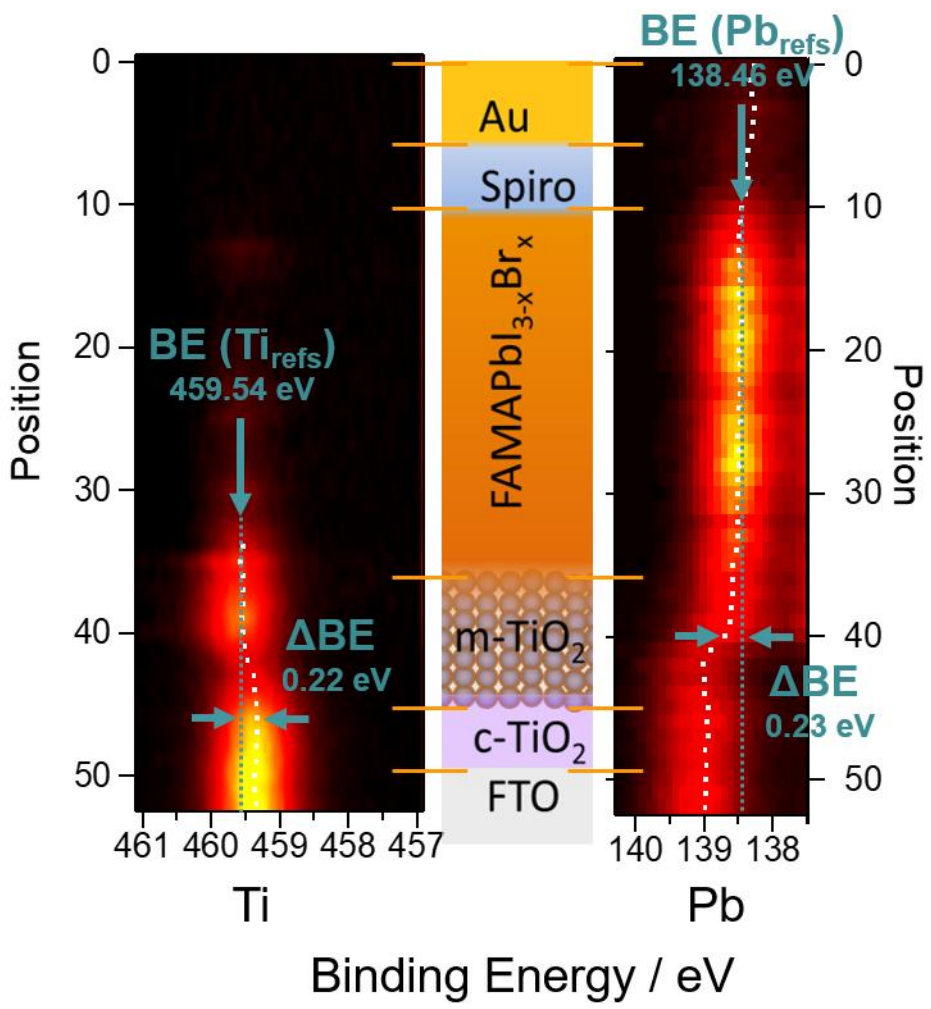

Figure S2: Intensity contour maps of the tapered cross-section line scans of the Ti 2p3/2 and Pb 4f7/2 core level spectra in dark. Binding energy shifts that should mimic chemical or electrostatic potential variation have been calculated and exemplified for position 46 – Ti and position 40 – Pb using respectively 459.54 eV and 138.46 eV as binding energy references. Reproduced with permission.[S1] Copyright 2020, John Wiley and Sons.

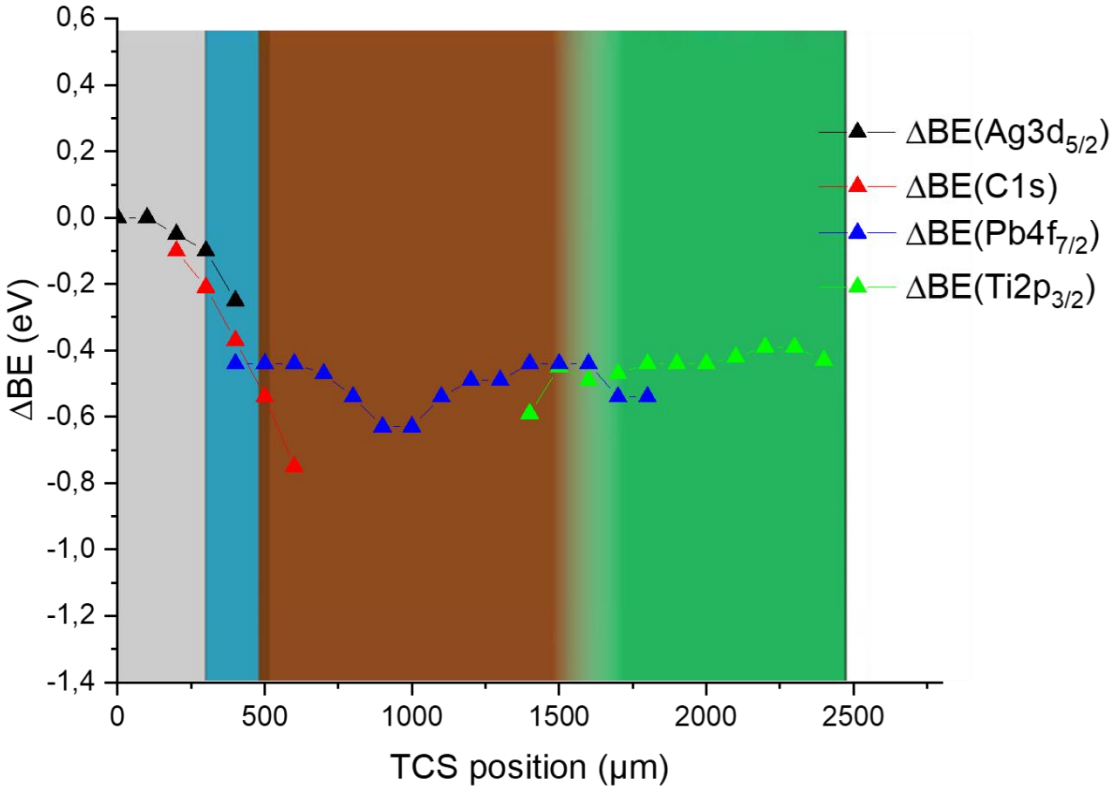

Figure S3: Electrostatic potential evolution over the Tapered cross-section of another perovskite solar cell. It was deduced from the TCS-PES measurements reported in previous work.[S2] The XPS line scan was only performed in dark. The experimental electrostatic potential evolution is the result of differences in binding energy (BE_{refs} - BE) for Ag3d5/2, C1s, Pb4f7/2, and Ti2p3/2 core levels for the contact layer (grey), the HTL (blue), the perovskite layer (brown) and for the ETL (green), respectively. Ag_{refs} = 368.05 eV, C_{refs} = 284.47 eV, Pb_{refs} = 138.44 eV, Ti_{refs} = 459.30 eV. For each new layer, the overall BE difference was used as a starting point for the next layer.

It can be noted that the interface between the Spiro-OMeTAD and the perovskite is not well-defined. Therefore, we chose to take -0.54 eV (binding energy shift of C1s at position 5) as a starting point for the $Pb4f_{7/2}$ shift.

It was a PSC with the following structure: Ag | Spiro-MeOTAD | $Cs_{0.05}(FA_{0.83}MA_{0.17})_{0.95}Pb(I_{0.83}Br_{0.17})_3$ | m-TiO_2 | c-TiO_2 | FTO. The TCS was created with a drilling machine, using a 2.0 mm conical polishing head and a low rotation speed. Then, a Thermo Fischer Scientific K-alpha system was used to perform PES. XPS line scans were acquired over the *tapered part* of the sample with a 100 µm distance between two positions.

An Al-Kα source (1486.6 eV) was used. The X-ray spot size was 50 x 50 µm^2. XPS measurements were performed every 50 µm of the 3 mm TCS. Reproduced with permission.[S2] Copyright 2021, John Wiley and Sons.

Table S1: Detailed simulation parameters used to compare with the measured, real device. Values that were found in the literature.[30–34]

Parameter	Value Real device	Comment
Temperature	300 K	
Work function of electron contact (FTO)	4.55 eV	
Work function of hole contact (Au)	5.1 eV	
Absorber Layer		
Generation rate (spatially homogeneous)	$4.8 \cdot 10^{21}$ cm^{-3}s^{-1}	
Thickness	300 nm	
Band gap energy	1.55 eV	
Relative dielectric permittivity	10	
Conduction band energy	4.0 eV	
Effective density of states in the conduction band	$5x10^{18}$ cm^{-3}	
Effective density of states in the valence band	$5x10^{18}$ cm^{-3}	
Recombination coefficient	10^{-10} cm^{3}s^{-1}	
Mobility of electrons	10 cm^2/(Vs)	
Mobility of holes	10 cm^2/(Vs)	
Shockley-Read-Hall lifetime	$2x10^{-8}$ s	
Electron-Transport-Layer (ETL) (TiO_x)		
Generation rate	0 cm^{-3}s^{-1}	
Thickness	50 nm	
Band gap energy	2.0 eV	
Relative dielectric permittivity	100	
Conduction band energy	4.4 eV	

Effective density of states of the conduction band	1.6×10^{19} cm^{-3}
Effective density of states of the valence band	1.6×10^{19} cm^{-3}
Mobility of electrons / holes	100 $cm^2/(Vs)$
n-Doping	10^{17} cm^{-3}

Hole-Transport-Layer (HTL) (Spiro-OMeTAD)

Generation rate	0 $cm^{-3}s^{-1}$
Thickness	100 nm
Band gap energy	3 eV
Relative dielectric permittivity	3
Conduction band energy	2.2 eV
Effective density of states of the conduction band	1.6×10^{19} cm^{-3}
Effective density of states of the valence band	1.6×10^{19} cm^{-3}
Mobility of electrons / holes	5×10^{-2} $cm^2/(Vs)$
p-Doping	10^{18} cm^{-3}

Section S2: Characteristics of the p-n-heterojunction and the n-n-heterojunctions:

Section S2.1: The p-n-heterojunction

Considering a p-n-heterojunction with material 1 on the left side that corresponds to Spiro-OMeTAD (Spiro) and material 2 on the right side that corresponds to perovskite it is assumed that the Spiro is p-doped with the concentration N_A and that perovskite is n-doped with the concentration N_D. $E_{\mathrm{C,i}}$, $E_{\mathrm{V,i}}$, $E_{g,i}$, and ε_i are their valence band edges, conduction band edges, bandgaps, and absolute permittivities, respectively.

From Semiconductor theory follows:

$$qV_{Bi} = E_{\mathrm{F},2} - E_{\mathrm{F},1} \tag{S2.1}$$

$$E_{\mathrm{F},2} - E_{\mathrm{C},2} = k_B T \ln\left(\frac{N_D}{N_{C,2}}\right) \tag{S2.2}$$

$$E_{\mathrm{V},1} - E_{\mathrm{F},1} = k_B T \ln\left(\frac{N_A}{N_{V,1}}\right) \tag{S2.3}$$

$$qV_{Bi} = E_{C,2} - E_{V,1} + k_B T \ln\left(\frac{N_A N_D}{N_{C,2} N_{V,1}}\right) \tag{S2.4}$$

$$qV_{Bi} = E_g - \Delta E_{C,(1-2)} + k_B T \ln\left(\frac{N_A N_D}{N_{C,2} N_{V,1}}\right) \tag{S2.5}$$

With the Schottky-Approximation:

$$\rho(x) = \begin{pmatrix} 0 & x_n < x \\ qN_D & 0 \le x \le x_n \\ -qN_A & x_p \le x \le 0 \\ 0 & x < x_p \end{pmatrix} \tag{S2.6}$$

the resulting electric field:

$$\boldsymbol{E}(x) = \begin{pmatrix} 0 & x_n < x \\ qN_D\,(x_n - x)/\,\varepsilon_2 & 0 \le x \le x_n \\ -qN_A(x - x_p)/\varepsilon_1 & x_p \le x \le 0 \\ 0 & x < x_p \end{pmatrix} \tag{S2.7}$$

and electrostatic potential

$$\phi(x) = \begin{pmatrix} q\frac{N_D x_n^2}{2\varepsilon_2} + q\frac{N_A x_p^2}{2\varepsilon_1} & x_n < x \\ -qN_D\,(x^2 - 2x x_n)/(2\,\varepsilon_2) + q\frac{N_A x_p^2}{2\varepsilon_1} & 0 \le x \le x_n \\ \frac{qN_A(x - x_p)^2}{2\,\varepsilon_1} & x_p \le x \le 0 \\ 0 & x < x_p \end{pmatrix} \tag{S2.8}$$

can be calculated.

From the result of the electrostatic potential

$$V_{Bi} = \frac{N_D x_n^2}{2\varepsilon_2} + \frac{N_A x_p^2}{2\varepsilon_1} \tag{S2.9}$$

and the need for charge neutrality

$$N_D x_n = N_A x_p \tag{S2.10}$$

The locations of the respective space charge regions can be calculated

$$-x_p = \sqrt{\frac{2\varepsilon_1\varepsilon_2 N_D}{qN_A}\frac{V_{Bi}}{\varepsilon_1 N_A+\varepsilon_2 N_D}} \tag{S2.11}$$

$$x_n = \sqrt{\frac{2\varepsilon_1\varepsilon_2 N_A}{qN_D}\frac{V_{Bi}}{\varepsilon_1 N_A+\varepsilon_2 N_D}} \tag{S2.12}$$

$$x_n - x_p = \sqrt{\frac{2\varepsilon_1\varepsilon_2}{q}\frac{(N_A+N_D)^2}{N_A N_D}\frac{V_{Bi}}{\varepsilon_1 N_A+\varepsilon_2 N_D}} \tag{S2.13}$$

$$x_n - x_p = \sqrt{\frac{2\varepsilon_1\varepsilon_2}{q^2}\frac{(N_A+N_D)^2}{N_A N_D}}\sqrt{\frac{E_g-\Delta E_{C,(1-2)}+k_B T\ln\left(\frac{N_A N_D}{N_{C,2}N_{V,1}}\right)}{\varepsilon_1 N_A+\varepsilon_2 N_D}} \tag{S2.14}$$

By looking at the derivative it can be seen that the space charge region increases with larger absolute permittivity

$$\frac{\partial W}{\partial \varepsilon_{1,2}} = \frac{\varepsilon_{2,1}N_{D,A}}{2\sqrt{\varepsilon_{1,2}}\left(N_{A,D}\varepsilon_{1,2}+N_{D,A}\varepsilon_{2,1}\right)^{3/2}} > 0 \tag{S2.15}$$

If we assume that the build-in field does not depend on the doping level, the space charge region increases with a larger built-in field

$$\frac{\partial W}{\partial V_{Bi}} > 0 \tag{S2.16}$$

If the doping level is already moderate that the additional charge carriers impact the width of the space charge region more than the increase in V_{Bi} the space charge region also decreases with additional doping. This can be easily verified with the following assumptions:

assuming $\frac{\partial V_{Bi}}{\partial N_{A,D}} \approx 0\ and\ N_A \approx N_D$ it follows straightforward:

$$\frac{\partial W}{\partial N_{A,D}} < 0 \tag{S2.17}$$

assuming $\frac{\partial V_{Bi}}{\partial N_{A,D}} \approx 0\ and\ \ \varepsilon_1 \approx \varepsilon_2$ it follows straightforward:

$$\frac{\partial W}{\partial N_{A,D}} < 0 \tag{S2.18}$$

For completeness' sake, it should be mentioned, that in the when going from an undoped homojunction to low doping, the space charge region initially increases because the difference in the fermi levels increases faster than the "shrinking" of the space charge region due to additional charge carriers. At a certain point the change in fermi level and therefore increase of the built-in field is slower than the shrinkage of the space charge region due to additional charge carriers.

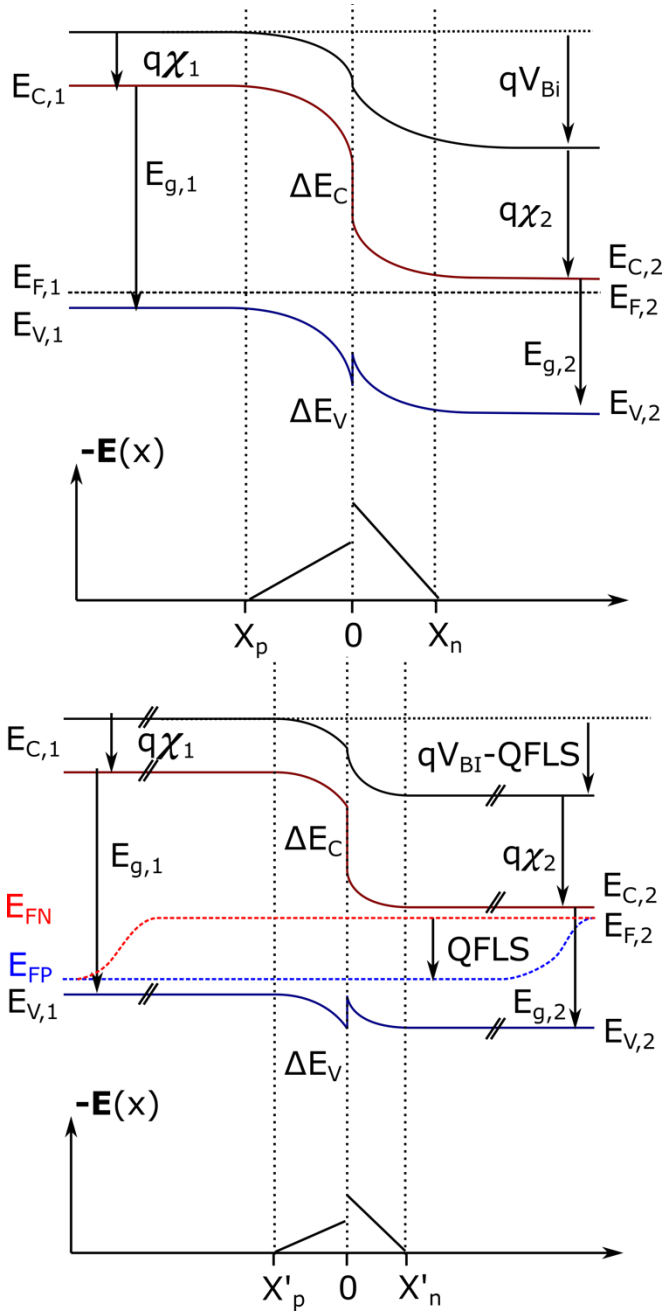

Figure S4: p-n-heterojunction band structure in the dark (top) and under illumination (bottom). A reduction in the built-in field can be observed due to illumination.

Section S2.2: The n-n-heterojunction

Considering a n-n-heterojunction with material 1 on the left side and material 2 on the right side. This would correspond to the PSC where the Perovskite is left and TiO_x right of the interface. It is assumed that the perovskite is n-doped with the concentration $N_{D,1}$ the conduction band edge is $E_{C,1}$, the valence band edge is $E_{V,1}$, the bandgap is $E_{g,1}$, and the absolute permittivity is ε_1. For the Perovskite it is assumed, that it is n-Doped with the

concentration $N_{D,2}$ the Conduction band edge is $E_{C,2}$, the Valence band edge is $E_{V,2}$, the Bandgap is $E_{g,2}$, and the absolute permittivity is ε_2.

For the built-in voltage it follows from semiconductor theory:

$$qV_{Bi} = E_{F,2} - E_{F,1} = \Delta E_{C,2-1} k_B T \ln\left(\frac{N_{D,2}}{N_{D,1}}\frac{N_{C,1}}{N_{C,2}}\right) \quad \text{(S2.19)}$$

Whereas the built-in field can be split into one part (ϕ_1) dropping over the depletion layer forming within the perovskite and the other part ϕ_2 dropping over the accumulation layer forming within the TiO_x.

$$V_{Bi} = \phi_1 + \phi_2 \quad \text{(S2.20)}$$

Solving the width of the accumulation layer is not analytically possible, but the depletion layer width can still be approximated.

$$\frac{qN_{D,1}x_n^2}{2\varepsilon_1} + \phi_2 = V_{Bi} \quad \text{(S2.21)}$$

It can be seen that the width of the depletion layer for an n-n junction correlates similarly with the material parameters as in a p-n junction. The differential equation governing the approximation region

$$\frac{d^2\phi_2}{dx^2} = \frac{q}{\varepsilon_2}\left(N_{D,2} - n(x)\right) = \frac{qN_{D,2}}{\varepsilon_2}\left(1 - exp(-\frac{q\phi_1}{k_B T})\right) \quad \text{(S2.22)}$$

cannot be analytically solved for the length of the accumulation region. However, the charge carrier density increases strongly towards the interface. It stands to reason that the dependency of the relevant length scale on material parameters is similar to the depletion region *i.e.* high doping concentration leads to a smaller accumulation region width.

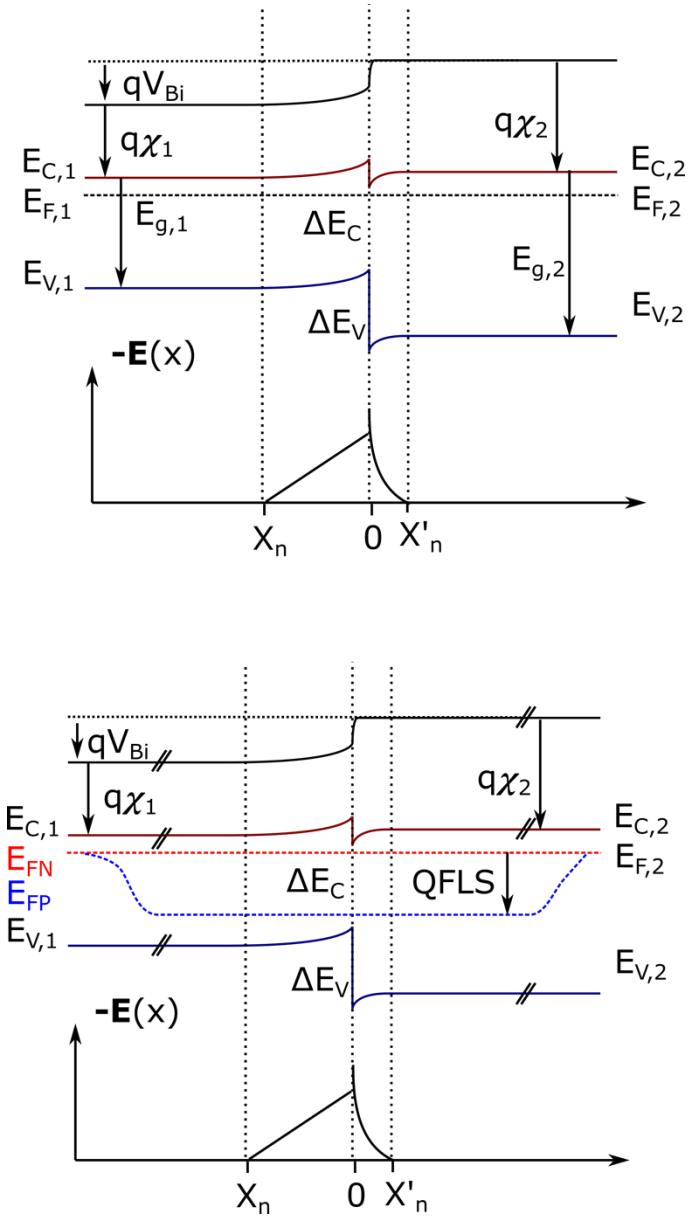

Figure S5: n-n-heterojunction band structure in the dark (top) and under illumination (bottom). No reduction in the built-in field can be observed due to illumination.

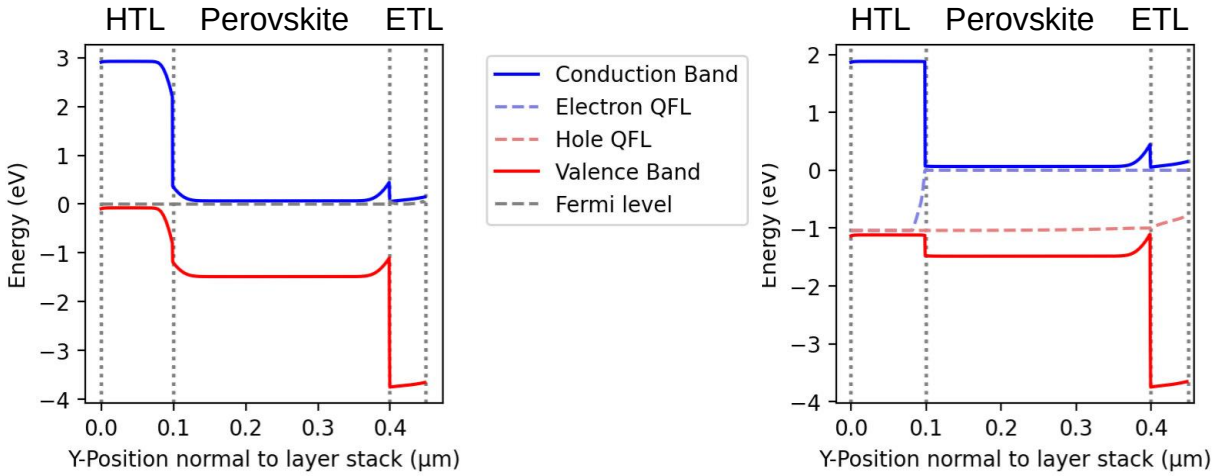

Figure S6: Resulting band structure in the dark (left) and under illumination (right) with the parameters reproducing the measurements of the TCS. Under illumination, the space charge region at the Spiro | perovskite interface is depleted leading to a reduced gradient in the conduction band and valence band. In the dark, the Fermi level is equal for holes and electrons, under illumination separate Quasi-Fermi levels for holes and electrons are used to parameterize the respective charge carrier density.

References:

S1. Wussler, M., Mayer, T., Das, C., Mankel, E., Hellmann, T., Prabowo, C., Zimmermann, I., Nazeeruddin, M.K., and Jaegermann, W. (2020) Tapered Cross-Section Photoelectron Spectroscopy of State-of-the-Art Mixed Ion Perovskite Solar Cells: Band Bending Profile in the Dark, Photopotential Profile Under Open Circuit Illumination, and Band Diagram. *Adv. Funct. Mater.*, **30** (27), 1910679.

S2. Das, C., Zia, W., Mortan, C., Hussain, N., Saliba, M., Ingo Flege, J., and Kot, M. (2021) Top-Down Approach to Study Chemical and Electronic Properties of Perovskite Solar Cells: Sputtered Depth Profiling Versus Tapered Cross-Sectional Photoelectron Spectroscopies. *Sol. RRL*, **5** (10), 2100298.